Copolar and Cross-Polar Radiation of Vivaldi Antenna on Dielectric Substrate

Benoît Stockbroeckx and André Vander Vorst, *Fellow, IEEE*

***Abstract*—The copolar and cross-polar radiation patterns of the Vivaldi antenna on a dielectric substrate are calculated and validated by measurements. The method involves a two-step procedure. The electric field distribution across the antenna slot aperture is calculated first. The radiated fields are then calculated, using Green's functions. The continuous exponential tapered shape is approximated by annular linearly tapered sections. The conical transmission-line theory and a variational method yield the electric field in each section. The radiation calculation is based on closed-form expressions for the dyadic Green's function of an elementary electric field source in a conducting half sheet. Both copolar and cross-polar radiation patterns of the Vivaldi antenna are calculated by integrating the Green's functions weighted by the electric field distribution over the antenna aperture. The effect of lateral truncation is taken into account by defining weighting patterns. The method is validated by original measurements and limitations of the model are discussed. Antenna directivity and sensitivity are calculated.**

***Index Terms*—Cross polarization, Vivaldi antennas.**

I. Introduction

In 1979, Gibson [1] has proposed the Vivaldi aerial as a new member of the class of frequency independent antennas. It is a traveling wave slot antenna having an exponentially tapered profile. The tapered slot antennas are traveling wave radiating devices, so that they are well suited for high operating frequencies (above 10 GHz), where a long electrical length is obtained with a reasonably short geometrical length. Applications of such traveling wave antennas have been reported up to 800 GHz [2]. Applications between 2–5 GHz have, however, been reported for array purposes [3]. The wide-band performance is impressive: the first reported application is a video receiver module for the frequency range of 8–40 GHz [1].

Several attempts to characterize the radiation properties of the Vivaldi antenna were empirical [1], [4], [5]. On the other hand, a full numerical analysis is proposed in [6], where the electromagnetic fields are computed by using the transmission line matrix (TLM) method inside of a rectangular box containing the antenna. The physical interpretation of the radiation mechanisms, however, is not obvious. Moreover, the full numerical approach is central processing unit (CPU) time consuming due to the large extent of the Vivaldi antenna.

In another approach, the current distribution on the antenna and the analytical asymptotic Green's function of a current element on the antenna are calculated separately. The closed-form expressions of Green's functions yield the physical interpretation of the radiation mechanisms (incident and diffracted fields). Their evaluation needs only a small CPU time. Interesting results are found in [7], where the Vivaldi antenna on a dielectric substrate is analyzed by a stepped approximation: the exponential taper is replaced by uniform slotline sections (Fig. 1). The propagation exponent and characteristic impedance are obtained for each section by applying Galerkin method, taking into account the transverse component of the electric field but not its curvature (Fig. 1). Consequently, the cross-polar radiated field cannot be calculated.

This approach is used in our method. We analyze the electric field distribution by approximating the continuous taper with annular linearly tapered slotline sections (Fig. 2). On each section, we apply a hybrid method [8] combining the conical transmission-line theory [9] and a fast variational method [10]. The conical transmission-line theory yields the azimuthal distribution, while the variational method accurately computes the longitudinal propagation exponent for each multilayered transmission-line section. Both the copolar and cross-polar radiated fields are calculated using closed-form expressions of Green's functions. The diffraction of the fields at the two lateral edges of the structure (edges **2** and **3** on Fig. 2) is taken into account as well. The method is validated by comparing the calculated radiation patterns with original measured values. The high- and low-frequency limits of the method are determined. Finally, the antenna directivity is calculated and the sensitivity analyzed.

II. Electric Field Distribution Calculation

We have shown that the linearly tapered-slot antenna in a homogeneous medium is a conical transmission line [8], [9]. The Vivaldi antenna (exponentially tapered-slot antenna) can be considered as a nonuniform conical transmission line. It can be decomposed into several conical transmission-line sections (Fig. 2). Slot-sector apex (X^{i}) and flare angle (φ_0^i) are different for each section since they correspond to different uniform conical slot lines. Consequently, the electric field distribution must be calculated for each conical transmission-line section.

The metallic parts of each section are described in the conical coordinate system while the dielectric substrate is described in the rectangular coordinate system. Hence, the electromagnetic fields in the inhomogeneous structure cannot be calculated by separating the variables. A hybrid method is then used: the azimuthal dependence is given by Lamé functions as described in [9] and the radial dependence is given by the propagation exponent of a uniform slotline having the local arc length as

Manuscript received November 30, 1998; revised October 5, 1999. This work was supported in part by the Government of the Walloon Region, Belgium, under the FIRST program.

The authors are with the Laboratoire d'Hyperfréquences, Université catholique de Louvain, B-1348 Louvain-la-Neuve, Belgium.

Publisher Item Identifier S 0018-926X(00)01274-6.

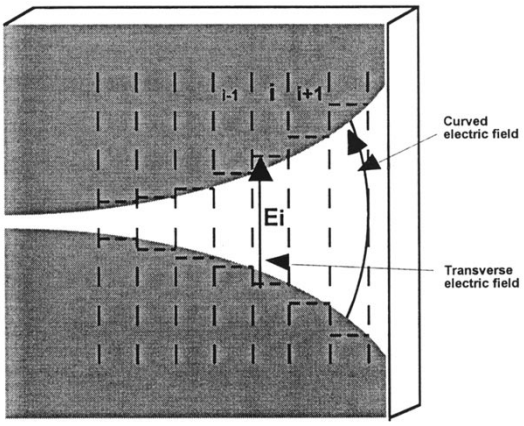

Fig. 1. Vivaldi antenna on dielectric substrate; taper truncation for field distribution analysis in [7]; electric field curvature and modeled transverse electric field.

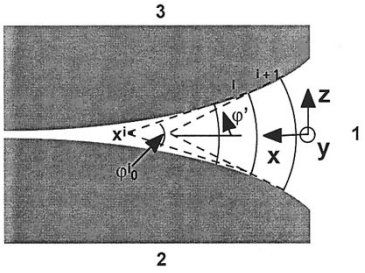

Fig. 2. Vivaldi antenna; annular taper truncation for field distribution analysis.

slot width. This complex propagation exponent is computed by the variational formulation developed in [10], taking the dielectric losses into account. Each conical slot-line section is characterized by its propagation exponent and characteristic impedance. The power continuity condition between two consecutive slot-line sections imposes that the electric field amplitude in section $i+1$ is larger than the one in section i by a factor $\sqrt{Z_c^{(i+1)}/Z_c^{(i)}}$, as in [7], $Z_c^{(i)}$ being the characteristic impedance of the ith section. The inverse proportionality to the radial distance from the source is meanwhile conserved, which takes the traveling wave radiation into account. The electric field distribution for the dominant mode in the ith section is consequently given as

$$E_{\varphi'}^{(i)} = \frac{E_0}{\sin\left(\frac{\varphi_0^{(i)}}{2}\right)} \frac{1}{\sqrt{1-\frac{\sin^2(\varphi')}{\sin^2\left(\frac{\varphi_0^{(i)}}{2}\right)}}} \cdot \sqrt{\frac{Z_c^{(i)}}{Z_c^{(i-1)}}} \frac{e^{-\gamma^{(i)}r'}}{r'} \tag{1}$$

where $\varphi_0^{(i)}$, $\gamma^{(i)}$, and $Z_c^{(i)}$ are the flare angle, propagation exponent, and characteristic impedance, respectively, of ith section. φ is the azimuthal angle bound to the slot sector (Fig. 2). The pole at $\varphi = \pm\varphi_0^{(i)}/2$ is the mathematical representation of the edge effect at the metallic edges of the ith sector. Dielectric losses are taken into account by using a complex propagation exponent. Conductor losses can be calculated by a perturbation method using the metal impedance. It is shown in [9] that the effect of those dielectric and conductor losses on the shape of the radiation patterns is negligible. They can, however, be non-negligible on the radiated power.

The main difference between the stepped approximation in [7] and our conical transmission-line approximation lies in the components of the electric field vector, which are considered across the aperture. In [7], the continuous taper is discretized into uniform slot-line sections so that the transverse component of the electric field is considered, while the longitudinal component due to the nonuniformity of the taper is not considered. In our analysis, however, the azimuthal component of the electric field is considered. It is decomposed into one transverse and one longitudinal component so that the curvature of the field is taken into account. Hence, the cross-polarized radiated field can be calculated by our method, which is an advantage.

III. Radiation Pattern

The azimuthal electric field across the slot (1) is decomposed into two components as

$$E_{\varphi'}\bar{\mathbf{a}}_{\varphi'} = \cos(\varphi')E_{\varphi'}\bar{\mathbf{a}}_z + \sin(\varphi')E_{\varphi'}\bar{\mathbf{a}}_x$$

where $\bar{\mathbf{a}}_z$ is the unit vector parallel to the edge and $\bar{\mathbf{a}}_x$ the unit vector perpendicular to the edge (Fig. 2). Using Green's formalism, the radiated fields are consequently

$$\overline{\mathbf{E}}^{(R)} = \iint_S E_{\varphi'}\overline{\overline{\mathbf{G}}} \cdot [\cos(\varphi')\bar{\mathbf{a}}_z + \sin(\varphi')\bar{\mathbf{a}}_x]\, dS \tag{2}$$

where S is the antenna aperture and $\overline{\overline{\mathbf{G}}}$ is the dyadic Green's function. Integral (2) has to be performed numerically. The analytical expression of Green's function is calculated in [11] for the copolar field in the E- and H-planes. We calculate it for both copolar and cross-polar fields for any direction [8]. Green's dyadic is given as

$$\overline{\overline{\mathbf{G}}} = \begin{pmatrix} G^{\theta,z} & G^{\theta,x} \\ G^{\varphi,z} & G^{\varphi,x} \end{pmatrix}$$

where $G^{\theta,z}$ and $G^{\theta,x}$ yield the copolar radiated field due to a longitudinal and a radial electric field source, respectively, while $G^{\varphi,z}$ and $G^{\varphi,x}$ yield the cross-polar radiated field due to a longitudinal and a radial electric field source, respectively. The closed-form expressions are

$$G^{\theta,z} = -\frac{e^{j(\pi/4)}}{\sqrt{2\pi}} \frac{e^{-jkr}}{r} k e^{jkz\cos\theta} \cdot \left\{ j|\sin\varphi| e^{jkx\sin(\theta)\cos(\varphi)} F[kx\sin(\theta)(1+\cos\varphi)] + \sin\left(\frac{\varphi}{2}\right) \frac{e^{-jkx\sin\theta}}{\sqrt{\pi kx\sin\theta}} \right\} \tag{3a}$$

$$G^{\theta,x} = 0 \tag{3b}$$

$$G^{\varphi,z} = -\frac{e^{j(\pi/4)}}{\sqrt{2\pi}}\,\frac{e^{-jkr}}{r}k\cos(\theta)e^{jkz\cos\theta} \cdot\left\{\pm j\cos(\varphi)e^{jkx\sin(\theta)\cos(\varphi)}F[kx\sin(\theta)(1+\cos\varphi)] + \cos\left(\frac{\varphi}{2}\right)\frac{e^{-jkx\sin\theta}}{\sqrt{\pi kx\sin\theta}}\right\} \tag{3c}$$

$$G^{\varphi,x} = \mp j\frac{e^{j(\pi/4)}}{\sqrt{2\pi}}\,\frac{e^{-jkr}}{r}k\sin(\theta)e^{jkz\cos\theta}e^{jkx\sin(\theta)\cos(\varphi)} F[kx\sin(\theta)(1+\cos\varphi)] \tag{3d}$$

where k is the wavenumber in free-space, (r,θ,φ) are the classical spherical coordinates and F is Fresnel's integral defined as

$$F(x) = \int_0^x \frac{e^{-jt}}{\sqrt{2\pi t}}\,dt.$$

It is shown in [7] that the two terms in (3a) and (3c) are related to one incident field and one diffracted field. The upper sign is chosen in (3c) and (3d) for the first two quadrants of φ and the lower sign for the last two quadrants.

The diffraction term in (3a) and (3c) shows that the diffracted electric field goes to infinity when the angle θ goes to zero or π. This is due to the edge effect when the observation point is close to the edge of the half sheet. In practical cases, the conductor half sheet is longitudinally finite, so that the edge effect does not physically occur for such critical angles. So, the factor $1/\sqrt{\sin\theta}$ is not taken into account. Moreover, the finiteness of the half sheet introduces two supplementary edges (Fig. 2, **2** and **3**) perpendicular to the main one (Fig. 2, **1**). Hence, the radiated field has to be modeled by considering the diffraction on the three edges. Diffraction on edges **2** and **3** highly affect the radiation pattern of the antenna when the distance between the slot and the edge is small, while it has no effect when the edges are far away from the taper. We have observed that the diffraction on edges **2** and **3** becomes significant when the length of edge **1** is shorter than two times the width of the aperture. There is, however, no analytical Green's functions available for such a three-edge geometry so that Green's functions (3a) and (3d) are used for the three edges separately. In such a way, each edge is considered as being the only one in the structure. This method yields, for each direction, three calculated values of the radiated field. These values have to be combined properly. The structure shows that the fields for θ close to zero, for example, are essentially affected by the diffraction on edges **1** and **3** and not affected by the diffraction on edge **2**. This observation is taken into account by defining a weighting pattern for each edge. These weighting patterns are defined as

$$F_w^{(1)} = \tfrac{1}{2}[1-\cos(\varphi)]$$
$$F_w^{(2)} = \tfrac{1}{2}[1-\cos(\theta)][1+\sin(\theta)\cos(\varphi)]$$
$$F_w^{(3)} = \tfrac{1}{2}[1+\cos(\theta)][1+\sin(\theta)\cos(\varphi)]$$

for edges **1**, **2**, and **3**, respectively. For example, the weighting pattern for edge **2** goes to zero for $\theta = 0$, as expected. Calculating the diffraction on edge **1** only is called here the one-edge diffraction method, while calculating the diffraction on edges **1**, **2**, and **3** and summing the weighted results is called the three-edge diffraction method.

One efficient method is proposed in [1] to reduce the diffraction on the side edges **2** and **3**. The authors make use of a corrugated structure etched at these edges. The effect of the dimensions of this structure on the radiation pattern of the antenna is presented in [13]. It is shown that the electric field amplitude at the edges is lowered due to the corrugated structure, which reduces the parasitic diffraction.

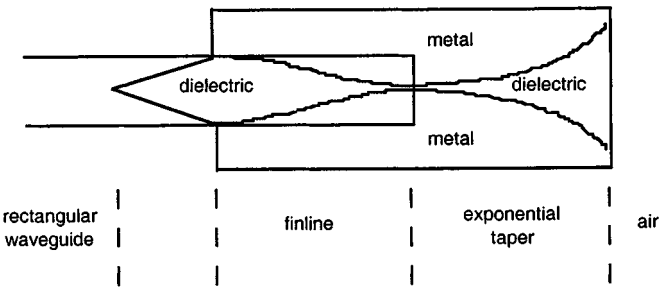

Fig. 3. Vivaldi antenna feeding structure for pattern measurements.

IV. Measurements, Validation, and Limitations

A. Measurements and Validation

Radiation patterns have been measured on different Vivaldi antennas. The antenna is inserted into a rectangular waveguide, which is slotted along its large side. The transition between the waveguide and the slotline is designed in view of a reduced return loss (Fig. 3): the dielectric substrate is cut in a quarter wavelength tapering and the metallic parts are introduced by a square sine taper to form a finline with a narrow slot (0.3 mm). As the slot is narrow, the fields are confined around it and the waveguide output is nearly transparent for them. The slotline is then exponentially tapered to form the Vivaldi antenna itself. The complete structure is fed by a Gunn diode cell at 24.125 GHz.

Simulation results are compared to measurements for a Vivaldi antenna etched on both sides of a dielectric substrate. Substrate relative permittivity is 3 and thickness is 0.508 mm. The operating frequency is 24.125 GHz. The tapered slotline width is expressed by the exponential function $s(z) = 0.3\,10^{-3}e^{102z}$, where z is the longitudinal position; s and z are in meters. Antenna length is 36 mm ($3\lambda_0$), slot width at the edge is 12 mm, and the metallic side parts are 4 mm wide. Such a small size for the metallic side parts does greatly affect the radiation patterns by nonnegligible diffraction on the two side edges. This is illustrated in the following figures.

Fig. 4 compares the measured and calculated copolar and cross-polar patterns in the plane $\varphi = 90°$, which is named here the V-plane (for vertical). The copolar main lobe is absolutely not accurate when calculated with the one-edge diffraction method: it is -17 dB below the measured level in the broadside direction ($\theta = 90°$). The three-edge diffraction method yields much better results. The cross-polar level also needs the three-edge diffraction rather than the one-edge diffraction. It is

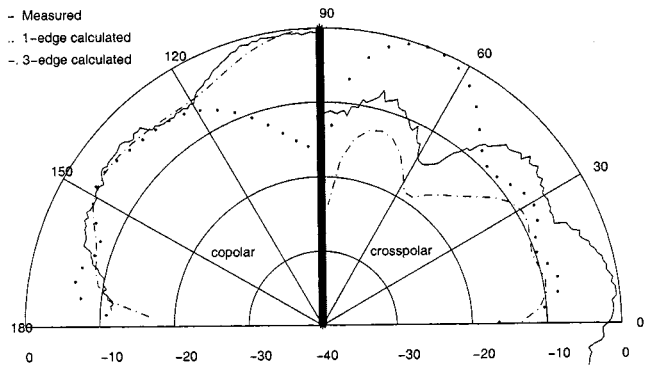

Fig. 4. Measured (−) and calculated (. and –.); V-plane ($\varphi = 90°$) radiation patterns; (.) one edge diffraction method; (–.) three edge diffraction method; copolar pattern (left) and cross-polar pattern (right); bilateral Vivaldi antenna with $\varepsilon_r = 3$, $d = 0.508$ mm; length 36 mm; taper exponent 0.102 mm-1; end-slot width 12 mm; metallic side-part width 4 mm; frequency 24.125 GHz.

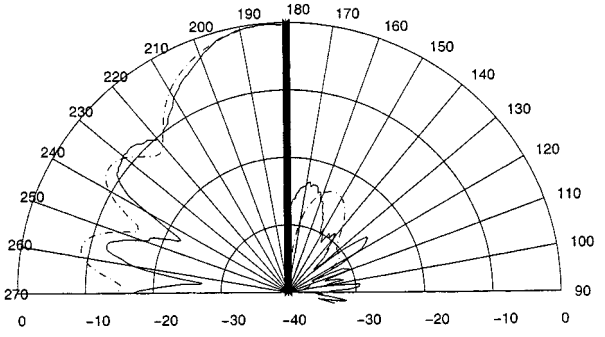

Fig. 5. Measured (–) and calculated (–.) H-plane ($\theta = 90°$) radiation patterns, three-edge diffraction method; copolar pattern (left) and cross-polar pattern (right); bilateral Vivaldi antenna with $\varepsilon_r = 3$, $d = 0.508$ mm; length 36 mm; taper exponent 0.102 mm-1; end-slot width 12 mm; metallic side-part width 4 mm;, frequency 24.125 GHz.

underestimated, however, with a few decibels. It appears that the cross-polar level is of the same order of magnitude as the copolar level in this plane and the simulation is confirmed by the measurements.

Fig. 5 compares the calculated (three-edge method) and measured patterns in the H-plane ($\theta = 90°$). The calculated copolar main lobe is accurate and the sidelobe levels at $\varphi = 230°$ and $255°$ are well predicted. The calculated sidelobe maximum is about 5° away from the measured maximum. We have shown that this is due to the combination of a not sufficiently accurate radial dependence calculation and a high-sensitivity of the H-plane pattern to that dependence [8]. This sensitivity is well known for any traveling wave antenna. By multiplying the calculated propagation exponent by a factor 1.05 (5% error), the measured and calculated maxima do coincide. The calculated propagation exponent is consequently underestimated. Because of symmetry, the cross-polar level is theoretically zero in the H-plane. As the pointing system on the measurement facility was not very precise, there is an uncertainty on the angle θ of the measured pattern and the cross-polar pattern has been measured in a slightly different plane. The cross-polar level is predicted accurately by imposing a small tilt of 2.25° in θ. Such an error on the antenna pointing is reasonable. This simulation is depicted on the right-hand side of Fig. 5.

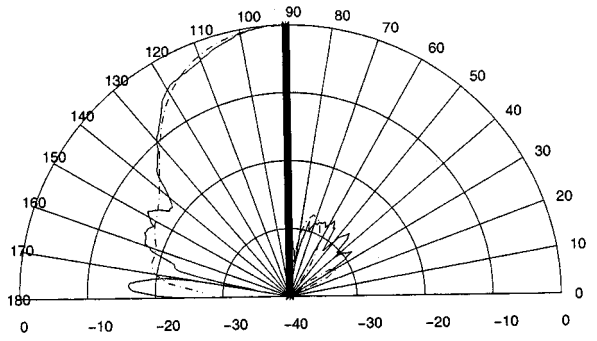

Fig. 6. Measured (–) and calculated (–.) E-plane ($\varphi = 180°$) radiation patterns, three edge diffraction method; copolar pattern (left) and cross-polar pattern (right); bilateral Vivaldi antenna with $\varepsilon_r = 3$, $d = 0.508$ mm; length 36 mm; taper exponent 0.102 mm-1; end-slot width 12 mm; metallic side-part width 4 mm; frequency 24.125 GHz.

Fig. 6 compares the measured and calculated (three-edge method) patterns in the E-plane ($\varphi = 180°$). The agreement is good for the copolar field. The measured cross-polar level is calculated accurately by imposing a small tilt of 1.8° on φ.

Fig. 7 compares results obtained by the three-edge diffraction method with measurements on a second Vivaldi antenna with a taper $s(z) = 0.3\,10^{-3}\ e^{154z}$. The antenna is shorter than the first one ($24\text{mm} = 2\lambda_0$) and etched on the same substrate. The calculated E-plane pattern is accurate except for the 3-dB beamwidth which is about 50° and 30° in the calculated and measured patterns respectively; the calculated 10-dB beamwidth is accurate (96°) and the calculated cross-polar level is good with a 2.4° tilt angle. The calculated H-plane 3-dB beamwidth is accurate and the 10-dB beamwidth is overestimated by about 25%, the calculated sidelobe level is overestimated by about 4 dB, and the calculated cross-polar level is good with a 1.8° tilt angle. The calculated V-plane pattern is very accurate. The calculated cross-polar level is somewhat underestimated by a few decibels with a tilt angle of 2.4°.

Better antenna performances have not been obtained by shaping the principal edge (**1**) as a curve so that the edge shape is matched to the curved electric field. Measurements have shown indeed that the patterns are the same as with the straight edge.

The Vivaldi antennas analyzed in Figs. 4–7 are made from a bilateral slotline excited with its even mode. We have shown [8] that theoretically, the parallel-plate mode is not excited below cutoff frequency $f_c = c_0/2d\sqrt{\varepsilon_r}$, where c_0 is the light speed in free-space, d is the substrate thickness, and ε_r its permittivity. The cutoff frequency is 170 GHz for the structures described in this section, so that parallel plate mode is not excited nor diffracted at the edges. Considering the case, however, of a tapered unilateral slot antenna etched on one side only of the dielectric substrate, at least TM_0 surface waves are always excited and propagated [14]. TM_0 surface waves have no cutoff frequency on such structures. We have shown that the surface wave is diffracted at the edges of the structure and that the radiation patterns are greatly affected [8]. The calculation method presented here does not take these surface waves into account so that it is generally not applicable to the unilateral antenna. One calculation method is proposed in [8] and [15] for the surface wave

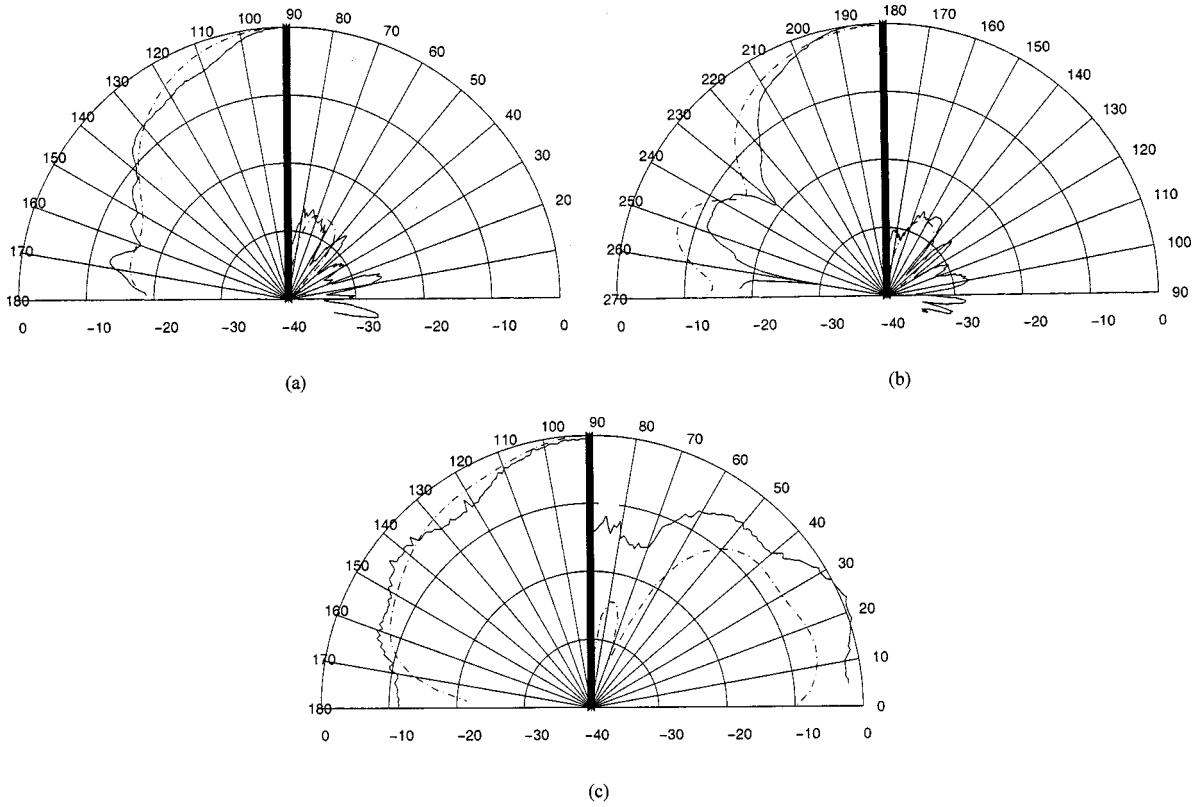

Fig. 7. Measured (–) and calculated (-.) radiation patterns; (a) E-plane, (b) H-plane, and (c) V-plane; three edge diffraction method; copolar pattern (left) and crosspolar pattern (right); bilateral Vivaldi antenna with ε_r = 3, d = 0.508 mm, length 24 mm, taper exponent 0.154 mm^{-1}, end slot width 12 mm, metallic side part width 4 mm, frequency 24.125 GHz.

diffraction calculation on unilateral structures. The surface wave amplitude, however, is low on very thin substrates so that they can be neglected and the calculation method presented here can be applied.

B. Limitations

The reflection of the propagating mode at the antenna edge has not been taken into account. It can be neglected indeed if the tapered slot is long enough in terms of the electrical length (at least $2\lambda_0$) and if the slot width at the edge is large enough (at least λ_0). Our model is consequently valid, for a given taper, for frequencies such that the wavelength is shorter than half the taper length and than the end-slot width. This observation introduces a low-frequency limit for our model.

We have shown [8] that the variational method [10] used in the hybrid analysis is not applicable when power leakage occurs between the bound mode and a surface wave mode. Such effect introduces a high-frequency limit, which depends on the substrate thickness and permittivity. Consequently, the model can be applied at submillimeter wavelengths provided the substrate is adequate.

V. Applications

The directivity has been computed by integrating the radiation pattern (Table I). The antenna taper is $s(z) = 0.3\,10^{-3}\ e^{102z}$ and the substrate is 0.508 mm thick with dielectric constant $\varepsilon_r = 3$. The directivity has been calculated for four antenna lengths equal to two, three, four, and five free-space wavelengths, respectively. The results yield a comparison of the one-edge diffraction method and the three-edge diffraction method. The directivity grows with the taper length for antennas shorter than 36 mm. It falls down dramatically for longer tapers. This is due to a path-length difference effect similar to that observed for horn antennas, which yields higher sidelobe levels and a local minimum in the endfire direction rather than the classical global maximum. The first three antenna directivities are lowered by about 1 dB by taking the lateral edge diffractions into account.

TABLE I
Bilateral Vivaldi Antenna
Directivity Versus Antenna Length for One-Edge Diffraction Method and Three-Edge Diffraction Method; $\varepsilon_r = 3$, $d = 0.508$ mm, $T = 0.102$ mm^{-1}, Frequency 24.125 GHz

Antenna length in mm	Directivity in dB 1-edge diffraction method	Directivity in dB 3-edge diffraction method
24	8.7	7.7
36	11.6	10.8
48	10.1	8.8
62.2	-14.1	-17.4

The sensitivity of the bilateral Vivaldi antenna radiation patterns to the working frequency is analyzed. Fig. 8 depicts the

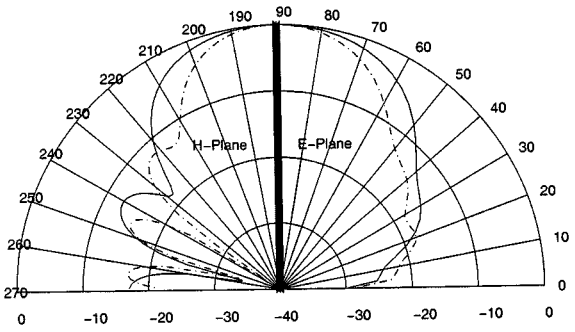

Fig. 8. Calculated radiation patterns; (–) 20 GHz and (–.) 30 GHz; H-plane (left) and E-plane (right); bilateral Vivaldi antenna with $L = 36$ mm, $\varepsilon_r = 3$, $d = 0.508$ mm, $T = 0.102$ mm^{-1}.

E- and H-plane radiation patterns for one Vivaldi antenna operating at 20 and 30 GHz. The antenna is 36 mm long, its taper profile is $s(z) = 0.3\,10^{-3}\ e^{102z}$, and the $\varepsilon_r = 3$ dielectric substrate is 0.508 mm thick. The 10-dB beamwidth variation is 28% in the H-plane and 26% in the E-plane for a 40% frequency variation. It illustrates the wide-band characteristics of the Vivaldi antenna on dielectric substrate. Three sidelobes are observed at 30 GHz, while only two are observed at 20 GHz. This is due to a longer electrical length at 30 GHz than at 20 GHz for the same geometrical length.

VI. Conclusion

The Vivaldi antenna is a nonuniform conical transmission line. We have calculated the electric field distribution by a hybrid method yielding the edge effect and curvature of the field with a small computation time for a multilayered structure. Both copolar and cross-polar radiated fields are calculated by using dyadic Green's functions corresponding to the perfectly conducting half sheet. Closed-form Green's functions are obtained, that are exact for far fields. The antenna edge is longitudinally finite in practical structures so that the diffraction due to two supplementary edges must be taken into account for correct modeling. This necessitates an appropriate definition for a weighting pattern for each edge. By combining the electric field distribution calculation and the closed-form Green's functions, the radiation pattern of any slot antenna made of conical slot-line sections can be calculated.

The accuracy of the copolar radiation patterns and cross-polar levels calculated by the present method is demonstrated by comparing with original measurements for two different bilateral Vivaldi antennas. The three-edge diffraction model is proved to be necessary for an accurate prediction of the measured patterns. The low-frequency limit of the method is when the wavelength is shorter than the taper half length and the end-slot width. The high-frequency limit is given by the leakage frequency. Under these restrictions, the method is applicable at submillimeter wavelengths.

The calculated antenna directivity grows with the antenna length, then falls down dramatically due to a phase difference effect. The directivity is lowered by about 1 dB by taking the lateral edge diffractions into account. The intrinsic wide-band characteristic of the Vivaldi antenna is illustrated by comparing the radiation patterns of one antenna calculated at two different frequencies (20 and 30 GHz).

Acknowledgment

The authors would like to thank R. Platteborze, P. Van averbeke, and the staff of BER s.a., Belgium, for their helpful assistance in setting up the measurement equipment.

References

[1] P. J. Gibson, "The Vivaldi Aerial," in *Proc. 9th Eur. Microwave Conf.*, Brighton, U.K., Sept.. 1979, pp. 101–105.

[2] P. R. Acharya, H. Ekström, S. S. Gearhart, S. Jacobsson, J. F. Johansson, E. L. Kollberg, and G. M. Rebeiz, "Tapered slotline antennas at 802 GHz," *IEEE Trans. Microwave Theory Tech.*, vol. 41, pp. 1715–1719, Oct. 1993.

[3] D. H. Schaubert, "Wide-band phased arrays of Vivaldi notch antennas," in *Proc. 10th Inst. Elect. Eng. Int. Conf. Antennas Propagat.*, Edinburgh, U.K., Apr. 1997, pp. 1.6–12.

[4] S. N. Prasad and S. Mahapatra, "A novel MIC slot-line antenna," in *Proc. 9th Eur. Microwave Conf.*, Brighton, U.K., Sept. 1979, pp. 120–124.

[5] T. Thungren, E. L. Kollberg, and K. S. Yngvesson, "Vivaldi antennas for single beam integrated receivers," in *Proc. 12th Eur. Microwave Conf.*, Helsinki, Finland, Sept. 1982, pp. 361–366.

[6] F. Ndagijimana, "Développement et application de la méthode TLM à l'étude des antennas dérivées de la ligne à fente," Ph.D. dissertation, INPG, Grenoble, France, 1990.

[7] R. Janaswamy and D. H. Schaubert, "Analysis of the tapered slot antenna," *IEEE Trans. Antennas Propagat.*, vol. AP-35, pp. 1058–1064, Sept. 1987.

[8] B. Stockbroeckx, "Space wave and surface wave radiation in the Vivaldi antenna," Ph.D. dissertation, Catholic Univ. Louvain, Louvain-la-Neuve, Belgium, 1998.

[9] B. Stockbroeckx and A. V. Vorst, "Electromagnetic modes in conical transmission line with application to linearly tapered slot antenna," IEEE Trans. Antennas Propagat., to be published.

[10] I. Huynen, D. Vanhoenacker, and A. V. Vorst, "Spectral domain form of new variational expression for very fast calculation of multilayered lossy planar line parameters," *IEEE Trans. Microwave Theory Tech.*, vol. 42, pp. 2099–2106, Nov. 1994.

[11] C.-T. Tai, *Dyadic Green Functions in Electromagnetic Theory*. New York: IEEE Press, 1994.

[12] S. Sugawara, Y. Maita, K. Adachi, K. Mori, and K. Mizuno, "A MM-wave tapered slot antenna with improved radiation pattern," in *Proc. IEEE MTT-S Int. Microwave Symp.*, Denver, CO, June 1997, pp. 959–962.

[13] ——, "Characteristics of a MM-wave tapered slot antenna with corrugated edges," in *Proc. IEEE MTT-S Int. Microwave Symp.*, Baltimore, MD, June 1998, pp. 533–536.

[14] B. Stockbroeckx and A. V. Vorst, "Asymptotic Green function of a surface magnetic current element on a perfect electroc conductor plane covered by a lossy dielectric substrate," *IEEE Trans. Antennas Propagat.*, vol. 47, pp. 309–316, Feb. 1999.

[15] B. Stockbroeckx, I. Huynen, and A. V. Vorst, "Effect of surface wave diffraction on the radiation pattern of a slot antenna etched in a finite ground plane," *Microwave Opt. Technol. Lett.*.

Benoît Stockbroeckx was born in Brussels, Belgium, in 1970. He received the E.E. and Ph.D. (applied sciences) degrees from the Université catholique de Louvain (UCL), Louvain-la-Neuve, Belgium, in 1993 and 1998, respectively.

In 1993, he joined the Microwave Laboratory at UCL. From 1993 to 1994 he investigated Yttrium Iron Garnet (YIG) resonators. His research interest is in microwave planar circuit modeling. Since 1994 he has been working on wide-band slot-line antenna and Vivaldi antenna modeling.

André Vander Vorst (M'64–SM'68–F'86) was born in Brussels, Belgium, in 1935. He received the Electrical and Mechanical Engineering degree from the Université catholique de Louvain (UCL), Belgium, in 1958, the M.Sc. degree in electrical engineering from the Massachusetts Institute of Technology (MIT), Cambridge, MA, in 1965, and the Ph.D. degree in applied sciences from UCL, in 1965.

He is currently with UCL, where he became an Assistant in 1958, an Assistant Professor in 1962, an Associate Professor in 1968, and a Professor in 1972. From 1958 to 1964 he worked on fast switching of magnetic cores. He was in the United States under a NATO fellowship from 1964 to 1966, first at MIT, then at Stanford University, Stanford, CA, both in the field of radio astronomy. In 1966, he founded the Microwave Laboratory at UCL, Belgium, which he is still heading. He has authored or coauthored three textbooks, several chapters, and a variety of scientific and technical papers in international journals and proceedings. He has been involved in all the research activities of the Laboratory, including loaded waveguides and cavities, atmospheric transmission and diffraction up to 300 GHz, designing and measuring active and passive circuits up to and above 100 GHz, and microwave bioelectromagnetics. His present interests include microwave-optical transducers, humanitarian demining, and the interaction of em fields with the nervous system.

Prof. Vorst was head of the Electrical Engineering Department (1970–1972), Dean of Engineering (1972–1975), Vice-President of the Academic Council (1973–1975), and President of the Open School in Economic and Social Politics (1973–1987), all at UCL, Belgium. He is a member of the National Committee of URSI and of various committees on communications, microwaves, and education. He has been active in IEEE Region 8 as well as in the European Microwave Conferences. He is a member of Academia Europaea and The Electromagnetics Academy. He received the Sitel Prize in 1986 and the Meritorious Service Award of the IEEE Microwave Theory and Techniques Society, in 1994.